

Revisiting the relation between the binding energy of finite nuclei and the equation of state of infinite nuclear matter

M. C. Atkinson^{1,2}, W. H. Dickhoff¹, M. Piarulli¹, A. Rios³, and R. B. Wiringa⁴

¹*Department of Physics, Washington University, St. Louis, Missouri 63130, USA*

²*Theory Group, TRIUMF, BC V6T 2A3, Canada*

³*Department of Physics, Faculty of Engineering and Physical Sciences, University of Surrey, Guildford, Surrey GU2 7XH, United Kingdom and*

⁴*Physics Division, Argonne National Laboratory, Argonne, Illinois 60439, USA*

(Dated: September 13, 2022)

The energy density is calculated in coordinate space for ^{12}C , ^{40}Ca , ^{48}Ca , and ^{208}Pb using a dispersive optical model constrained by all relevant data including the corresponding energy of the ground state. The energy density of ^8Be is also calculated using the Green's function Monte-Carlo method employing the Argonne/Urbana two and three-body interactions. The nuclear interior minimally contributes to the total binding energy due to the $4\pi r^2$ phase space factor. Thus, the volume contribution to the energy in the interior is not well constrained. The dispersive-optical-model energy densities are in good agreement with *ab initio* self-consistent Green's function calculations of infinite nuclear matter restricted to treat only short-range and tensor correlations. These results call into question the degree to which the equation of state for nuclear matter is constrained by the empirical mass formula. In particular, the results in this paper indicate that saturated nuclear matter does not require the canonical value of 16 MeV binding per particle but only about 13-14 MeV when the interior of ^{208}Pb is considered.

I. INTRODUCTION

The investigation of the binding energy of atomic nuclei dates back to the origins of nuclear physics [1]. The well-known empirical mass formula, developed by Bethe and Weizsäcker [2, 3], accurately describes the global aspects of nuclear binding for most of the nuclear chart. Its success is largely due to the saturating nature of the constituent nucleons in nuclei. The evidence for nuclear saturation came from measurements of the root-mean-squared (rms) charge radius of nuclei which revealed that the volume of a given nucleus scales linearly with A [1, 4]. Elastic electron-scattering experiments revealed that the density in the interior of nuclei saturates at a value around $\rho_0 \approx 0.16 \text{ fm}^{-3}$ [4, 5]. In order to understand the mechanism behind nuclear saturation, infinite nuclear matter (NM) is an ideal system that is often studied [6–8]. Depending on the method and realistic nucleon-nucleon (NN) interaction used, the calculated value of ρ_0 in NM can stray from the experimental value as discussed *e.g.* in Ref. [9]. In addition to the density at saturation, the associated binding energy, E_0 , plays a vital role in the equation of state (EOS) of NM. The EOS does not exhibit saturation in neutron-rich systems, but its characterization is nonetheless relevant for astrophysical research on supernovae and neutron stars [10–12].

The traditional method used to estimate ρ_0 is fundamentally different than that of E_0 . While the value of ρ_0 is determined experimentally, E_0 is determined empirically from an extrapolation of the empirical mass formula [4, 13, 14]

$$BE(A, Z) = -a_V A + a_S A^{2/3} + a_C Z(Z-1)A^{-1/3} + \frac{1}{2} a_A (A - 2Z)^2 A^{-1}, \quad (1)$$

where a_V , a_S , a_C , and a_A are parameters fit to nuclear masses [1]. Because the only link between Eq. (1) and NM is the volume term, the canonical value of the saturation energy is assumed to be $E_0/A = -a_V \approx -16 \text{ MeV}$ [4, 13]. However, this involves a significant extrapolation that neglects proper consideration of long-range correlations (LRC) in both finite and infinite systems [6, 15–17]. Contributions to the binding energy from LRC are associated with collective phenomena. In finite nuclei, these emerge as low-lying natural parity surface vibrations and higher-lying giant resonances. These excitations are associated with the presence of a surface and therefore have no counterpart in NM. Conversely, LRC in NM are characterized by their total momentum (and spin-isospin quantum numbers) which have no direct counterpart in finite nuclei as momentum is not a good quantum number of an excited state in a nucleus. This is particularly problematic for matter excitations with pionic quantum numbers as the related soft mode in NM occurs at finite momentum and thereby contributes substantially to binding, is strongly enhanced by the coupling to the Δ -isobar, and increases in importance with density. For this reason, it was argued in Ref. [15] that the link between finite nuclei and NM saturation properties should be confined to the effect of short-range correlations (SRC). Assumptions made about the role of LRC therefore influence the link between finite nuclei and nuclear matter. As will be shown below, it is possible to establish such a link using the *ab initio* method of self-consistent Green's functions (SCGF). We therefore propose to exercise caution when equating a fundamental property of NM to a parameter that relies heavily on the chosen functional form of the empirical mass formula.

The mass formula of Eq. (1) is built upon the liquid drop model (LDM) of finite nuclei. The LDM has been

studied and modified several times. These modifications mainly involved accounting for deformation, shell effects, and pairing. A recent form of the LDM, known as the finite-range droplet model, has improved agreement with experimental masses [18]. Additionally, there have been many other macroscopic mass models such as that of Duflo-Zuker [19], Koura [20], and others (see Ref. [18] for a review of mass models). The parameters of Eq. (1) have also been analyzed using different methods of statistical analysis resulting in errors in the range of 0.03 - 0.24 for a_V [21]. Much work has been focused on the parameters of Eq. (1), but not the connection between a_V and E_0 . While all nuclear mass models like Eq. (1) show good agreement with experimental masses, none address the issue of the contribution of LRC as discussed above.

To further explore the extrapolation from the LDM to NM, consider the analogous infinite system of liquid Helium. Quantum Monte Carlo studies of drops of atomic Helium, both bosonic ^4He [22] and fermionic ^3He [23] using the HFDHE2 atom-atom interaction [24], are able to extract a reasonable volume binding energy from finite drops in a liquid drop mass formula only by including additional terms beyond the standard volume and surface terms of Eq. (1). For the ^3He case, fitting the energies of drops containing up to 240 atoms with only volume and surface terms predicts a volume binding energy of -1.42 K while adding a curvature term $\propto A^{1/3}$ generates a much better fit with a volume term of -2.09 K. This is much closer to the infinite liquid result of -2.36 K and the experimental value of -2.47 K. The extrapolated energy of the infinite system is highly dependent on the chosen functional form of the LDM. The discrepancy between the experimental binding energy and the volume energy of the LDM for liquid ^3He indicates that the traditional extrapolation to an infinite system is insufficient even for a system with only a simple central interaction.

An alternative connection between the physics of finite nuclei and that of NM is provided by energy density functionals (EDFs) used in nuclear density functional theories (DFTs). The EDF provides a one-to-one correspondence between binding energy and density based on effective forces such as Skyrme or Gogny. These EDFs are parametrized by fits and used to self-consistently solve for the ground state density of nuclei with Kohn-Sham (or Hartree-Fock) type equations [25]. A result of these calculations is a nucleus-dependent energy density profile which is used to calculate the total binding energy. These more microscopic approaches are very successful in calculating binding energies and other properties across the nuclear chart [25]. The value of E_0 can be calculated directly from the EDF parameters. However, in the vast majority of Skyrme and Gogny EDFs, E_0 is a parameter of the fit rather than a prediction (or extrapolation) from properties of finite nuclei [26–28]. Thus, density functionals reproduce the canonical value of E_0 by construction.

In the present paper we discuss various ingredients that address some of the issues related to determining

the saturation point of symmetric NM and re-examine the empirical value of E_0 . This is done by comparing three different methods of obtaining the value of E_0 : the canonical value obtained from an empirical mass formula extrapolation (a_V), the minimum energy in NM from *ab initio* SCGF simulations, and the energy density in the interior of finite nuclei based on the dispersive optical model (DOM). In Sec. II, we present results from DOM calculations of several nuclei that are constrained, in addition to scattering observables, by ground-state properties including the energy. By casting these results in terms of an energy density, we show in Sec. III that it is possible to make contact with *ab initio* SCGF calculations of symmetric and asymmetric nuclear matter [9, 29]. The DOM ground-state energy is calculated using the Migdal-Galitski sum rule, so it does not explicitly include three-body forces [30]. We address this issue by utilizing energy densities from Monte Carlo calculations obtained using various chiral two- and three-body interactions [31–33] as well as the phenomenological Argonne/Urbana combination [34]. Further analysis of DOM nuclear energy densities is presented in Sec. IV before the conclusions in Sec. V.

II. DISPERSIVE OPTICAL MODEL APPROACH

Ideally, a sound determination of E_0 would rely on a NM theoretical calculation based on the true NN interaction (*i.e.* obtained as a solution of the quantum chromodynamics Lagrangian). In practice, calculations of the saturation point of NM are hampered by approximations in the NN forces, limited by the treatment of three-nucleon (NNN) interactions, and display a substantial dependence on the employed many-body method [9, 35–37]. This scheme dependence ultimately undermines a direct, reliable determination of E_0 . Moreover, this approach is not directly related to experimentally verifiable properties of energy densities in finite nuclei.

Alternatively, we investigate the connection between the empirical mass formula and the value of E_0 through energy densities calculated using the DOM. This method constrains a complex self-energy $\Sigma_{\ell j}$ using both scattering and bound-state data [38, 39]. The self-energy is a complex and nonlocal potential that unites the nuclear structure and reaction domains through dispersion relations [38–40]. The Dyson equation generates the single-particle propagator, or Green's function, $G_{\ell j}(r, r'; E)$ from which bound-state and scattering observables can be deduced. Results of DOM fits of ^{12}C , ^{40}Ca , ^{48}Ca , and ^{208}Pb are considered here.

Traditionally, DOM fits are constrained by quasihole energies, particle numbers, charge densities, and, because of the dispersion relation, by all relevant scattering data up to 200 MeV. Here, we extend the treatment to incorporate also the total binding energy of each nucleus as obtained from the Green's function. A position-dependent

energy density within the nucleus can then be defined such that its volume integral is the total binding energy. This approach provides a novel determination of nuclear energy densities based entirely on experimental data. Unlike mean-field or DFT energy densities, this approach is not constrained by prescribed analytics on energy densities. DOM fits produce occupation numbers that are not step-like, hence the corresponding kinetic-energy densities are not of a free-Fermi gas nature. Moreover, these energy densities can be used to relate the energy of these nuclei to SCGF calculations in NM that only treat the consequences of SRC while including full off-shell propagation [9, 29].

The binding energy of a nucleus can be expressed as the expectation value of the Hamiltonian using the full A -body wave function, $E_0^A = \langle \Psi_0^A | \hat{H} | \Psi_0^A \rangle$. The energy density, $\mathcal{E}_A(r)$, of a nucleus can then be defined such that

$$E_0^A = \int d^3r \mathcal{E}_A(r) = 4\pi \int_0^\infty dr r^2 \mathcal{E}_A(r). \quad (2)$$

The energy of the ground state can be recast into the Migdal-Galitski sum rule [30] for both proton and neutron contributions with $E_0^A = E_0^N + E_0^Z$ [6]. Since the DOM is calculated in a coordinate-space basis of Lagrange functions [41], $\mathcal{E}_A(r)$ can be calculated using

$$\mathcal{E}_A(r) = \frac{1}{2} \int_0^{\varepsilon_F} \sum_{\ell j} (2j+1) \left[E S_{\ell j}^h(r, r; E) + \int_0^\infty dr' r'^2 \langle r | \hat{T}_\ell | r' \rangle S_{\ell j}^h(r', r; E) \right] dE, \quad (3)$$

where \hat{T}_ℓ is the kinetic-energy operator in the partial-wave basis and $S_{\ell j}^h(r, r'; E)$ is the hole spectral function,

$$S_{\ell j}^h(r, r'; E) = \frac{1}{\pi} \text{Im} G_{\ell j}^h(r, r'; E).$$

The first term corresponds to a combination of the kinetic- and potential-energy densities [6] while the second term represents the kinetic-energy density

$$\mathcal{T}(r) = \sum_{\ell j} (2j+1) \mathcal{T}_{\ell j}(r),$$

where

$$\mathcal{T}_{\ell j}(r) = \int_0^{\varepsilon_F} dE \int_0^\infty dr' r'^2 \langle r | \hat{T}_\ell | r' \rangle S_{\ell j}^h(r', r; E).$$

The volume integral of $\mathcal{T}(r)$ is the total kinetic energy of the nucleus. The kinetic-energy operator in coordinate space,

$$\langle r | \hat{T} | r' \rangle = \delta^3(\mathbf{r} - \mathbf{r}') \frac{-\hbar^2 \nabla_r^2}{2\mu}$$

is used to calculate $\mathcal{T}(r)$, resulting in the following expression:

$$r^2 \mathcal{T}_{\ell j}(r) = \frac{-\hbar^2}{2\mu} \left[\frac{d^2}{dr^2} - \frac{\ell(\ell+1)}{r^2} \right] [r n_{\ell j}(r, r') r'] \Big|_{r'=r},$$

TABLE I. Comparison of the DOM calculated binding energies of ^{12}C , ^{40}Ca , ^{48}Ca , and ^{208}Pb calculated using Eq. (3) to those calculated using the empirical mass formula. We use the parameters $a_V = 15.6$, $a_S = 17.2$, $a_C = 0.697$, and $a_A = 46.6$ (all in MeV) in Eq. (1). The experimental binding energies are shown in the last column. All listed energies are in MeV.

A	DOM E_0^A/A	Mass Eq.	Exp. E_0^A/A
^{12}C	-7.32	-7.29	-7.68
^{40}Ca	-8.46	-8.50	-8.55
^{48}Ca	-8.66	-8.59	-8.66
^{208}Pb	-7.76	-7.81	-7.87

where $n(r)$ is the one-body density matrix defined as

$$n_{\ell j}(r, r') = \int_0^{\varepsilon_F} dE S_{\ell j}^h(r, r'; E).$$

It is important to note that this derivation assumes there are no three-body terms in the nuclear interaction [42]. The presence and need of a nuclear three-body force is undisputed [43], but the arguments below do not change in any essential way by the assumption that Eq. (3) can be treated as exact (see Sec. III for further discussion). In particular, we will show that Variational Monte Carlo (VMC) calculations leading to exact Green's function Monte Carlo results (GFMC) [44] require only a modest attractive three-body contribution to the binding energy of light nuclei. With chiral interactions [45], the three-body force is important to generate NM saturation, but the many different versions hamper uniform conclusions and their softness may yield interior densities that are too large [46].

With Eq. (2), the binding energy of nuclei are also included in DOM fits with an accuracy of about 1.5% and shown for ^{12}C , ^{40}Ca , ^{48}Ca , and ^{208}Pb in Table I. Details of the ^{12}C DOM fit are presented in the Appendix while details for ^{40}Ca , ^{48}Ca , and ^{208}Pb fits can be found in Refs. [47–49], respectively. The agreement with experiment in Table I is of a similar quality to that obtained by an empirical mass-formula fit. However, the DOM also reproduces the experimental charge densities, indicating that the hole spectral functions are well constrained.

The energy density of ^{40}Ca , weighted by the volume element $4\pi r^2$, and its separation in kinetic- and potential-energy density are shown in Fig. 1. The weighting is chosen to emphasize the parts of the energy density that contribute to the integral in Eq. (2). The figure clearly illustrates that the interior of the nucleus has a suppressed importance for the total energy on account of the phase space factor. The nucleon point-density is shown in addition to the energy densities in Fig. 1 to demonstrate that the radial dependence of the energy density, $\mathcal{E}_A(r)$, and of the actual matter density, $\rho(r)$, are very similar. We explore this point further in the following section.

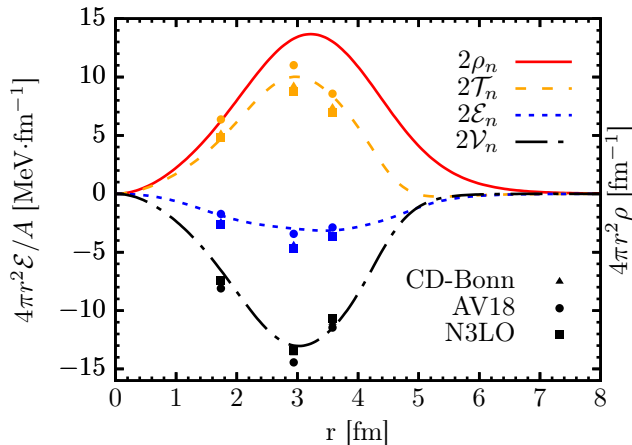


FIG. 1. The energy density of ^{40}Ca calculated from the DOM using Eq. (3). Each line corresponds to twice the contribution from neutrons (see text). The curves correspond to the energy density (dotted line), kinetic-energy density (dashed line), potential-energy density (dot-dashed line), and nucleon point-density (solid line). All curves are weighted by a volume element $4\pi r^2$. The points are taken from a SCGF calculation in NM for three different interactions based on Ref. [29] at densities corresponding to 0.08, 0.12, and 0.16 fm^{-3} .

III. COMPARISON WITH *AB INITIO* CALCULATIONS

SCGF calculations in NM from Ref. [29] are represented by symbols in Fig. 1. Each different symbol corresponds to a different NN interaction in the SCGF calculation, where the triangles correspond to the charge-dependent Bonn (CD-Bonn) interaction [50], the circles correspond to the Argonne v_{18} (AV18) interaction [51], and the squares correspond to the Idaho next-to-next-to-next-to-leading order (N3LO) chiral interaction [52]. The calculation in NM is for specific values of the nuclear density which are mapped to radii using the DOM matter density. These results cannot be directly compared to the energy density in finite nuclei because there is no Coulomb force included in NM. Since there are an equal number of protons and neutrons in ^{40}Ca , isospin symmetry implies that their distributions would be the same if the Coulomb force were ignored. Thus, using twice the neutron energy density in ^{40}Ca is an effective way of removing the influence of the Coulomb force. This is how the lines in Fig. 1 are generated. These isospin-corrected results provide energy densities that are similar to those predicted by SCGF calculations with very different NN interactions. The agreement with the NM calculations is striking since the latter only include effects of short-range (SRC) and tensor correlations as suggested in Ref. [15]. This implies that the interior of ^{40}Ca exhibits NM-like properties.

The momentum content in the DOM analysis is substantially larger than typical predictions of mean-field (EDF) calculations. For instance, the DOM kinetic-

energy density in ^{40}Ca peaks at a value of around $\approx 10 \text{ MeV fm}^{-1}$. Skyrme EDF kinetic-energy densities generated using the HFBRAD code [53], not shown here for brevity, have peaks in the range $\approx 6.5 - 7.5 \text{ MeV fm}^{-1}$. The unambiguous presence of high-momentum nucleons, as experimentally probed in Ref. [54], documents the need for such an enhanced momentum content. Such enhancements are also obtained in the results of SCGF calculations illustrated in Fig. 1. We stress that DOM fits are not separately constrained on the kinetic- and potential-energy (density) contributions. In other words, the sizes of the kinetic and potential energy densities are dictated by data, but agree extremely well with the theoretical SCGF calculations for NM.

In particular, the interaction with the best agreement with the DOM energy density in Fig. 1 is AV18. It is interesting that, unlike the other two interactions, the harder AV18 correctly reproduces the nuclear saturation density $\rho_0 \approx 0.16 \text{ fm}^{-3}$ [4, 13] in the SCGF calculation reported in Ref. [9], but saturates at about -11.5 MeV . This is in disagreement with the canonical value, $a_V \approx -16 \text{ MeV}$, which comes from the empirical mass formula. However, it is clear from Fig. 1 that the interior of the nucleus does not determine the binding energy since it minimally contributes to Eq. (1). Concurrently, it is apparent that SCGF calculations in NM generate quantitatively correct binding as shown in Fig. 1. As discussed above, the interior of the nucleus saturates around ρ_0 , implying that this region corresponds to saturated NM. This is further supported by the reproduction of the smooth interior charge density in the DOM. We therefore draw three conclusions. First, with the interpretation that NM is representative of the core of finite nuclei, we infer that there is no strong constraint that the binding energy of NM has to be a_V . Second, the agreement between the NM points and ^{40}Ca in Fig. 1 is consistent with the fact that SRC are primarily what link finite nuclei to NM [15–17]. Third, we conjecture that the AV18 interaction with $E_0 \approx -11.5 \text{ MeV}$ produces consistent results not only for the density at saturation, but also the energy when compared to the interior of ^{40}Ca .

This conjecture is empirically supported by the fact that the AV18 + Urbana-IX [34] (3-body interaction) was used to derive the Akmal, Pandharipande, and Ravenhall (APR) EOS of nuclear matter [12]. It is widely used in calculations of neutron star structure, all of which are consistent with current observations of neutron stars including the recent neutron star merger event [12, 55]. The APR EOS correctly predicts the value of ρ_0 but with a minimum energy of $E_0 = -12.6 \text{ MeV}$. While the value of this minimum energy has been seen as a defect of the APR EOS, its success in describing nuclear systems further supports a saturation energy different from a_V .

The fact that the binding energy density traces the matter density in Fig. 1 is not surprising when considering the decomposition of the binding energy using full

A -body wave functions,

$$\begin{aligned} E_0^A &= \langle \Psi_0^A | \hat{H} | \Psi_0^A \rangle = E_0^A \langle \Psi_0^A | \Psi_0^A \rangle \\ &= E_0^A \int d^3 r_1 \left[\int d^3 r_2 \dots d^3 r_A |\Psi_0^A(\mathbf{r}_1, \mathbf{r}_2, \dots, \mathbf{r}_A)|^2 \right], \end{aligned} \quad (4)$$

where the complete set $\{|\mathbf{r}_1, \mathbf{r}_2, \dots, \mathbf{r}_A\rangle\}$ has been inserted and all other quantum numbers are suppressed for clarity. Noting that the bracketed term in Eq. (4) is the one-body density distribution $\rho(\mathbf{r})$, the binding energy can be written as

$$E_0^A = \frac{E_0^A}{A} \int d^3 r \rho_A(\mathbf{r}) \implies \mathcal{E}_A(r) = \left(\frac{E_0^A}{A} \right) \rho_A(r). \quad (5)$$

Eq. (5) is not a unique expression of the energy density since only its integral (the binding energy) is an observable. However, Eq. (5) is a natural choice because the energy densities in Fig. 1 roughly trace the matter density. While Eq. (5) is exact, it cannot be used as a replacement for Eq. (3) because there is no guarantee that the DOM propagator is equal to the exact propagator, which would be built from the exact A -body ground-state wave function [6].

A method that is well-suited to calculate the energy density using Eq. (4) is GFMC. The results of a corresponding GFMC calculation for the ^8Be binding-energy density is shown in Fig. 2, generating a total kinetic energy of 239 MeV, a two-body potential energy of -287 MeV, a three-body potential energy of -10.7 MeV, and a total energy of -56.1 MeV compared to the experimental value of -56.5 MeV. In this calculation, the AV18 + Urbana-X [56] (UX) interactions were employed to generate the ground-state wave function. The results in Fig. 2 include the contribution of the three-body interaction to the energy density. Comparing the two- and three-body potential density clarifies that the latter contributes mod-

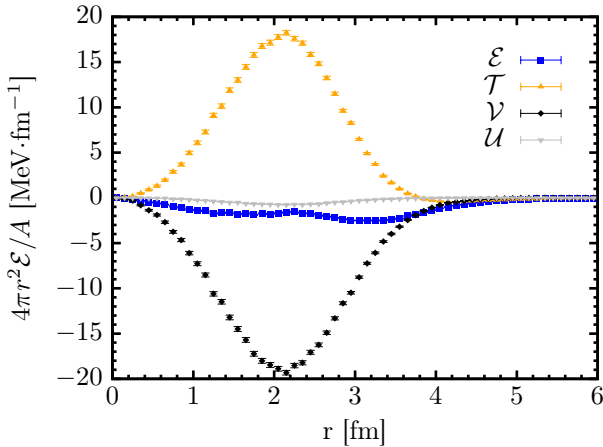


FIG. 2. Results of a GFMC calculation of ^8Be with \mathcal{E} , \mathcal{T} , \mathcal{V} , \mathcal{U} , and \mathcal{V}_C representing the total energy, the kinetic energy, the two-body potential energy, the three-body potential energy, and the Coulomb energy density, respectively.

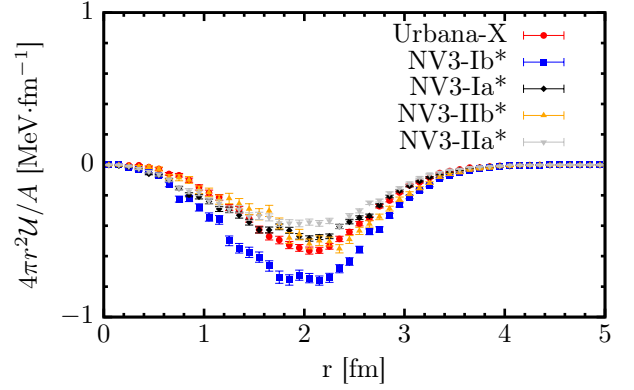


FIG. 3. Illustration of the 3-body potential energy densities for different chiral interactions [31] and the UX [56] for ^{12}C .

estly to the total energy density and certainly is not capable of changing its shape. Consequently, we expect that ignoring the three-body interaction by using Eqs. (2) and (3) in the DOM analysis will not alter the shape of the binding-energy density.

In order to further assess the effects of the NNN interaction, we also report VMC calculations of ^{12}C using the three-body components (NV3*) of the Norfolk chiral interactions (NV2+3*) [31–33] as well as the UX NNN interaction. In Fig. 3, we show the three-body potential densities calculated in ^{12}C using these five different interactions. In particular, NV3* models have been constrained by fitting the trinucleon energies and the empirical value of the Gamow-Teller matrix element in tritium β decay in combination with the corresponding Norfolk two-body potential (NV2). There are two classes (I and II) of NV2, differing only in the range of laboratory energy over which they are fitted to the nucleon-nucleon database; class I up to 125 MeV, and class II up to 200 MeV. For each class, two combinations of short- and long-range regulators have been used, namely $(R_S, R_L) = (0.8, 1.2)$ fm (models NV2-Ia and NV2-IIa) and $(R_S, R_L) = (0.7, 1.0)$ fm (models NV2-Ib and NV2-IIb). In Table II, we explicitly report the potential energy contributions to the binding energy of ^{12}C using the interactions displayed in Fig. 3. Again, we find that the contributions from NNN forces to the total energy (density) are small in comparison to the corresponding NN ones. As

TABLE II. Potential energy contributions from the NNN (and corresponding NN) interactions shown in Fig. 3 for ^{12}C .

Interaction	V	U
AV18+UX	-457	-10.5
NV2+3-Ib*	-383	-15.9
NV2+3-Ia*	-379	-10.3
NV2+3-IIb*	-416	-10.4
NV2+3-IIa*	-411	-8.91

expected, there is some variation in the NNN potential densities for the different interactions used. However, the

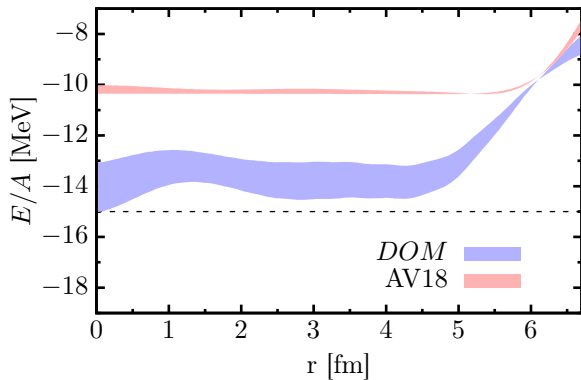


FIG. 4. Binding energy as a function of radius in ^{208}Pb . The thick blue band covers the range of energies of ^{208}Pb calculated using the DOM matter density (top) and the use of the DOM proton density scaled by 208/82 (bottom), both with Coulomb removed. The narrow band is similarly obtained from the SCGF calculations for the AV18 [29] (see text). The dashed line is the expected energy from the empirical mass formula.

fact that these variations are small demonstrates that, regardless of the NNN interaction used, the shape of the binding-energy density is not altered in a significant way by NNN forces. In all cases, the NNN potential-energy-density contribution is small in comparison with the corresponding NN one.

IV. ANALYSIS

The nuclear energy density can be further explored for the heavier nuclei ^{48}Ca and ^{208}Pb . The agreement between Eq. (5) and Eq. (3) in ^{48}Ca and ^{208}Pb is comparable to that of ^{40}Ca . The case of ^{208}Pb is particularly interesting because the interior is more extended than in ^{40}Ca and ^{48}Ca . This implies that finite-size (surface) effects are reduced in this region of ^{208}Pb , making it an even more suitable system to compare with NM. Using isospin symmetry to remove the effect of the Coulomb interaction on the energy density of ^{40}Ca is not valid in ^{208}Pb , since $N > Z$. While removing the Coulomb energy density from $\mathcal{E}(r)$ would provide a NM-like energy density, the Coulomb potential is still reflected in the matter density of ^{208}Pb (see also Ref. [49]). One way to compare with the NM calculations for asymmetric matter from Ref. [29] is to completely remove the Coulomb potential from the DOM self-energy. To preserve the proton number, the proton Fermi energy must therefore be shifted such that it remains between the particle-hole gap of the protons. The resulting Coulomb-less matter density exactly confirms the expected 0.16 fm^{-3} in the interior of ^{208}Pb .

The energy in the interior can be approximately cal-

culated from the energy density using Eq. (5),

$$E_A(r) \approx \mathcal{E}_A(r) \left(\frac{A}{\rho_A(r)} \right).$$

This approximation should be valid for small values of r , where the nuclear density is relatively constant and saturated. The binding energy with Coulomb removed as a function of r in ^{208}Pb is shown in Fig. 4. The ambiguity to determine the Coulomb-less interior density is reflected in the wide band. The thin band represents the interpolation of SCGF calculations from Ref. [29] using AV18 at densities corresponding to 0.08, 0.12, and 0.16 fm^{-3} obtained in the same way. These NM results require an additional 2-3 MeV per particle attraction to reproduce the DOM result, which is not inconsistent with the trend obtained for the required contribution of the three-body interaction to accurately describe the energies of light nuclei with GFMC [43]. The contribution of the symmetry energy per nucleon from the empirical mass formula in ^{208}Pb is $E_{\text{sym}} = 1.04\text{ MeV}$, leading to the expectation of the interior energy of ^{208}Pb to be $E_0^{208} = -15.0\text{ MeV}$ based on the empirical mass formula (see dashed line in Fig. 4). Our analysis therefore suggests that the energy in the interior (and hence the saturation energy) is less bound than what is expected from the empirical mass formula. In ^{208}Pb , we find $E_A/A \approx -14\text{ MeV}$.

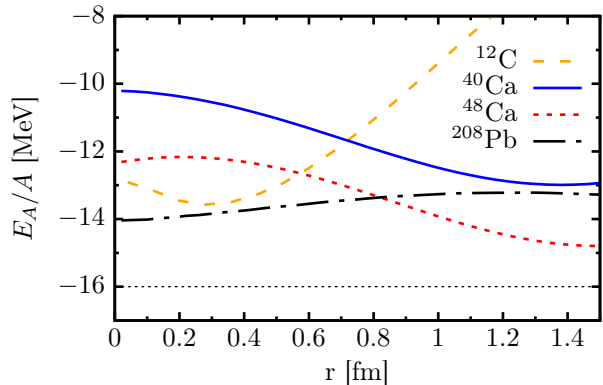


FIG. 5. Binding energy as a function of radius in ^{12}C (dashed line), ^{40}Ca (solid line), ^{48}Ca (dotted line), and ^{208}Pb (dot-dashed line). The latter reflects the middle of the band in Fig. 4. The canonical -16 MeV/A binding is also shown.

A comparison of the DOM energy as a function of radius for ^{12}C , ^{40}Ca , ^{48}Ca , and ^{208}Pb is shown in Fig. 5, where the Coulomb contribution has been removed from each nucleus. The energies in the core of each nucleus are all within a few MeV of each other. Near the origin, all of them are significantly less bound than 16 MeV per particle. We expect that this result holds across a wide range of isotopes. It also appears to be robust to statistical uncertainties in the DOM fits and, as discussed above, to the (relatively small) contribution of NNN forces. We take this as a strong hint that the central energy density departs significantly from the canonical value obtained

via the a_V parameter of mass formulae.

V. CONCLUSIONS AND OUTLOOK

The interpretation that the interior of the nucleus is a close approximation to NM implies that a macroscopic mass formula, such as Eq. (1), is not a suitable way of determining the binding energy of NM at saturation. Our results invalidate this approach by shedding light on two different aspects. First, Fig. 1 clearly shows that the interior of the nucleus does not significantly contribute to the total binding energy. Nuclear masses should thus only have small contributions from the saturated, deep nuclear interior. In other words, mass formulae are unlikely to capture the energy dynamics of the nuclear interior, including its mass number dependence. Second, the interior saturation energies, as shown by the DOM analysis above, do not necessarily agree with the value of a_V that provides a good fit to nuclear masses. It has been noted in the past [15–17] that LRC in finite nuclei and nuclear matter are not commensurate, implying an uncertainty in the extrapolation from Eq. (1) to NM. Taking our results into consideration leads to the inevitable conclusion that the saturation energy of symmetric NM is less than the canonical value of 16 MeV per particle. Considering the interior of ^{208}Pb indicates that E_0 is actually closer to 13–14 MeV. This is also closer to the value generated by SCGF calculations of NM with the AV18 force.

These results can also be interpreted in terms of different energy values that are traditionally expected to be similar. On the one hand, a_V quantifies the bulk mass-number dependence of nuclear masses. On the other, the saturation energy of NM, E_0 , provides the minimum energy of an infinite system. Mass-number fits are however performed on finite nuclei data and thus extrapolations to the $A \rightarrow \infty$ limit need to be considered with care [57]. Experience with other many-body systems like Helium drops indicates that one may be able to shift contributions of different A -dependent terms within mass formulae, thus changing the value of a_V . Our analysis in fact suggests that the value of E_0 may be about 10% smaller than that obtained from a_V . It remains to be seen whether mass formulae with lower values of a_V provide quantitative fits to nuclear masses.

To our knowledge, the systematic uncertainty in the value of E_0 extrapolated from a_V has not been investigated since the construction of Eq. (1). With the development of more precise NN interactions as well as the continued improvement of many-body methods, it is important to have an accurate value of the nuclear saturation point. This is often used in benchmarking NN and NNN forces [37]. In fact, modern chiral NN interactions already incorporate nuclear observables, such as binding energies and charge radii of nuclei, to their fitting protocols [58]. It has been suggested that the NM saturation point should also be added to these fits [35]. In light of this and the conclusions of this article, it is imperative

that new methods of determining the value and uncertainty of E_0 are explored.

We suggest a way forward in connecting E_0 to nuclear observables. Rather than relying uniquely on bulk masses, we use the energy density in the nuclear interior, $E_A(\rho)$, to provide an estimate for E_0 . The energy density is accessible by several contemporary many-body methods. Here, for instance, we have used quantum Monte Carlo simulations in light nuclei to validate the DOM predictions and gauge the importance of different components to the energy density. This has helped confirm that the contribution of NNN is relatively small. A similar analysis could be performed with other *ab initio* methods that can reach higher masses and even compute NM within the same footing [35]. This would provide a theory-to-theory connection between the saturation point of NM and the properties of nuclei.

Our results also suggest that in addition to purely theoretical methods, nuclear data can also provide an insight into the energy density profile within nuclei. The unified view of nuclear scattering data and bound properties obtained from the DOM is in fact able to provide a quantitative description of the nuclear energy density. In this first exploratory work, we have not dealt explicitly with NNN forces, but some steps in this direction could be easily explored in conjunction with similar many-body methods like the SCGF approach. Extending the DOM fits to other isotopes across the nuclear chart will also provide a further quantitative, nuclear-data-inspired understanding of the mass evolution of nuclear energy densities.

ACKNOWLEDGEMENT

The work of MCA and WHD was supported by the U.S. National Science Foundation under grants PHY-1613362 and PHY-1912643, the work of AR by the UK Science and Technology Facilities Council (STFC) through grant ST/P005314/1, the work of RBW by the U.S. Department of Energy, Office of Nuclear Physics under contract DE-AC02-06CH11357 and the NUCLEI SciDAC program, with computational resources provided by the Argonne Laboratory Computing Resource Center, and the work of MP by the U.S. Department of Energy funds through the FRIB Theory Alliance award DE-SC0013617 with computational resources provided by the Argonne Leadership Computing Facility via the 2019/2020 ALCC “Low energy neutrino-nucleus interactions” for the project NNInteractions.

Appendix A: Parametrization of the potentials

The parametrization and fit of ^{12}C is presented in this appendix. The parametrizations of ^{40}Ca , ^{48}Ca , and ^{208}Pb can be found in Refs. [47–49], respectively. Table III displays the parameters for the ^{12}C self-energy.

The constraint of the number of particles was incorporated to include contributions from $\ell = 0$ to 10. Such a range of ℓ -values generates a sensible convergence with ℓ when short-range correlations are included as in Ref. [59]. We obtain 5.8 protons from all $\ell = 0$ to 10 partial wave terms including $j = \ell \pm \frac{1}{2}$ and 5.9 for neutrons. The corresponding binding energy can be found in the main text.

We found the DOM self-energy by minimizing the χ^2 using experimental data in the form of elastic-scattering cross sections, total and reaction cross sections, charge density, and particle number. The resulting elastic-scattering cross sections are shown in Fig. 6, the proton analyzing powers are shown in Fig. 7, the proton reaction cross section is shown in Fig. 8, and the neutron total cross section is shown in Fig. 9. The charge density is shown in Fig. 10.

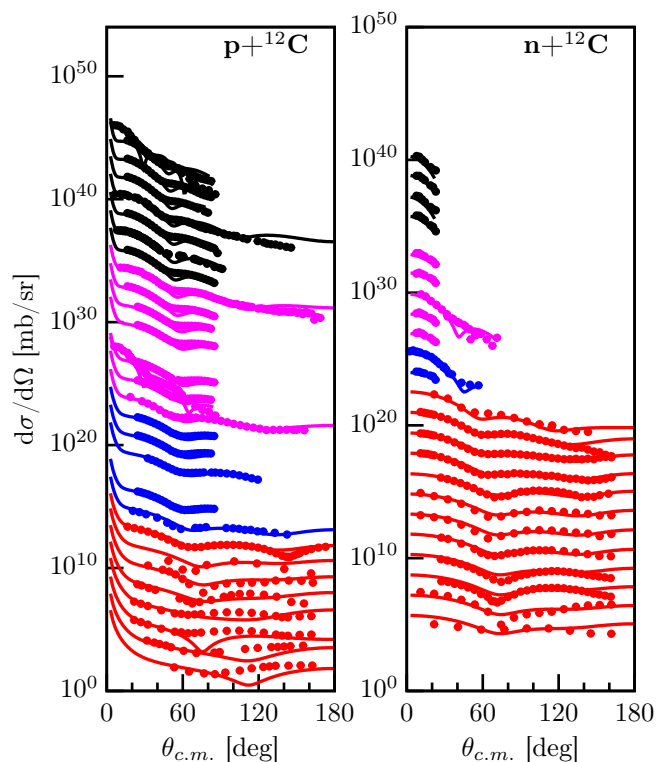


FIG. 6. Calculated and experimental proton and neutron elastic-scattering angular distributions of the differential cross section $\frac{d\sigma}{d\Omega}$ at energies ranging up to 200 MeV. The data at each energy is offset by factors of ten to help visualize all of the data at once. Refs. [60–78] contain the proton experimental data. Refs. [79–85] contain the neutron experimental data.

REFERENCES

-
- [1] A. Bohr and B. R. Mottelson, *Nuclear Structure: Volume I* (World Scientific, 1997).
 - [2] H. A. Bethe and R. F. Bacher, *Rev. Mod. Phys.* **8**, 82 (1936).
 - [3] C. F. v. Weizsäcker, *Zeitschrift für Physik* **96**, 431 (1935).
 - [4] H. A. Bethe, *Annu. Rev. Nucl. S.* **21**, 93 (1971).
 - [5] R. Hofstadter, *Ann. Rev. Nucl. S.* **7**, 231 (1957).
 - [6] W. H. Dickhoff and D. Van Neck, *Many-Body Theory Exposed!, 2nd edition* (World Scientific, New Jersey, 2008).
 - [7] K. A. Brueckner, C. A. Levinson, and H. M. Mahmoud,

TABLE III. Fitted parameter values for proton and neutron potentials in ^{12}C .

Parameter	Value
Hartree-Fock	
V^{HF} [MeV]	90.8
r^{HF} [fm]	0.952
a^{HF} [fm]	0.417
β^{vol_1} [fm]	0.908
β^{vol_2} [fm]	0.738
x	0.911
ρ^{wb} [fm]	1.01
β^{wb} [fm]	0.0251
Spin-orbit	
V^{so} [MeV]	26.6
r^{so} [fm]	0.540
a^{so} [fm]	0.755
β^{so} [fm]	1.23
A^{so} [MeV]	-1.62
B^{so} [MeV]	66.4
Volume imaginary	
a_+^{vol} [fm]	0.536
r_+^{vol} [fm]	1.27
β_+^{vol} [fm]	0.340
a_-^{vol} [fm]	0.256
r_-^{vol} [fm]	1.02
β_-^{vol} [fm]	1.08
A_+^{vol} [MeV]	6.51
B_+^{vol} [MeV]	25.3
\mathcal{E}_+^{vol} [MeV]	2.31
A_-^{vol} [MeV]	16.9
B_-^{vol} [MeV]	8.97
\mathcal{E}_-^{vol} [MeV]	1.61
\mathbb{E}_+ [MeV]	23.4
\mathbb{E}_- [MeV]	67.5
α	0.189
Surface imaginary	
a_+^{sur} [fm]	0.493
r_+^{sur} [fm]	1.40
β_+^{sur} [fm]	3.38
a_-^{sur} [fm]	0.316
r_-^{sur} [fm]	0.631
β_-^{sur} [fm]	1.72
A_+^{sur} [MeV]	13.0
$B_+^{sur_1}$ [MeV]	26.3
$B_+^{sur_2}$ [MeV]	198
C_+^{sur} [MeV]	199
A_-^{sur} [MeV]	28.0
$B_-^{sur_1}$ [MeV]	23.11
$B_-^{sur_2}$ [MeV]	20.0
C_-^{sur} [MeV]	94.9

- Phys. Rev. **95**, 217 (1954).
 [8] H. A. Bethe, Phys. Rev. **103**, 1353 (1956).
 [9] M. Baldo, A. Polls, A. Rios, H.-J. Schulze, and I. Vidaña, Phys. Rev. C **86**, 064001 (2012).
 [10] C. J. Horowitz and J. Piekarewicz, Phys. Rev. Lett. **86**, 5647 (2001).
 [11] A. W. Steiner, J. M. Lattimer, and E. F. Brown, The Astrophysical Journal **722**, 33 (2010).

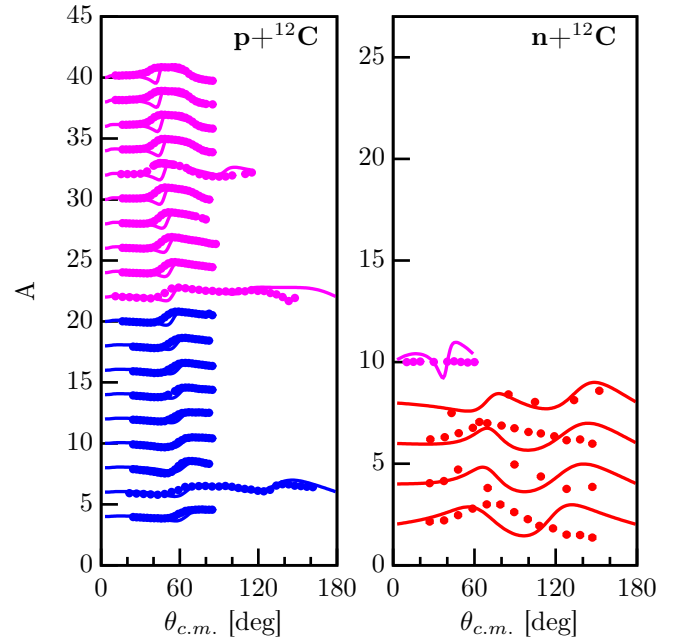


FIG. 7. Calculated and experimental proton and neutron analyzing powers at energies ranging up to 200 MeV. Refs. [66, 69, 74, 86–89] contain the proton experimental data. Refs. [80, 90, 91] contain the neutron experimental data.

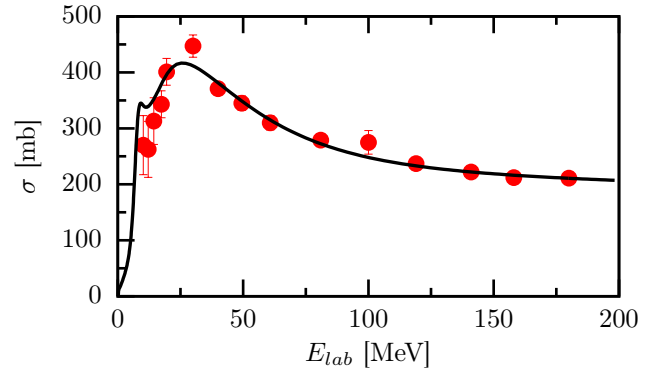


FIG. 8. Proton reaction cross section generated from the DOM self-energy. The experimental data can be found in Refs. [92–94].

- [12] A. Akmal, V. R. Pandharipande, and D. G. Ravenhall, Phys. Rev. C **58**, 1804 (1998).
 [13] W. Myers and W. Swiatecki, Nuclear Physics A **601**, 141 (1996).
 [14] J. P. Jeukenne, A. Lejeune, and C. Mahaux, Physics Reports **25**, 83 (1976).
 [15] Y. Dewulf, W. H. Dickhoff, D. Van Neck, E. R. Stoddard, and M. Waroquier, Phys. Rev. Lett. **90**, 152501 (2003).
 [16] W. H. Dickhoff and C. Barbieri, Progress in Particle and Nuclear Physics **52**, 377 (2004).
 [17] W. H. Dickhoff, Journal of Physics: Conference Series **702**, 012013 (2016).
 [18] D. Lunney, J. M. Pearson, and C. Thibault, Rev. Mod. Phys. **75**, 1021 (2003).

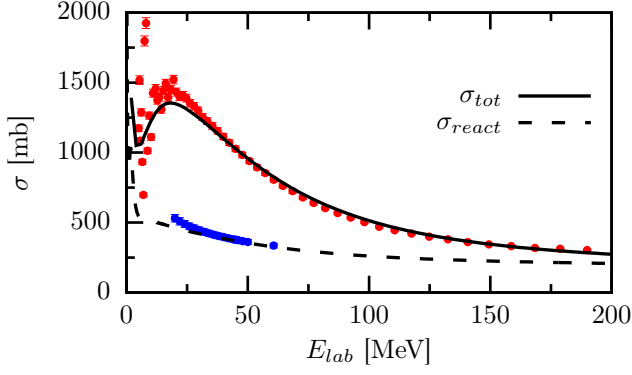


FIG. 9. Neutron total cross section (solid line) and reaction cross section (dashed line) generated from the DOM self-energy. The total cross section data can be found in Ref. [95]. The reaction cross section data can be found in Ref. [96].

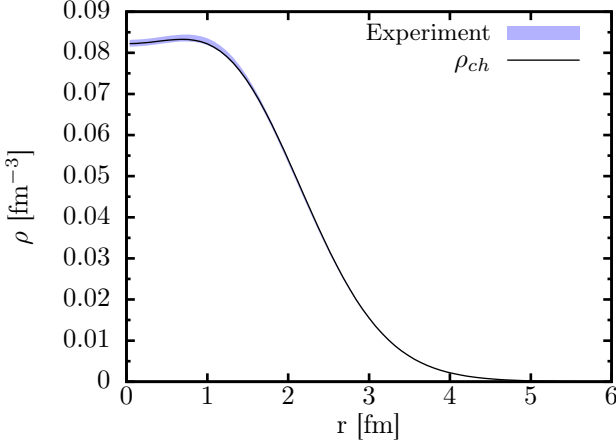


FIG. 10. Experimental and fitted ^{12}C charge density. The solid black line is calculated using the DOM self-energy and folding with the proton charge distribution while the experimental band represents the 1% error associated with the extracted charge density from elastic electron scattering experiments using the sum of Gaussians parametrization [97, 98].

[19] J. Duflo and A. Zuker, *Phys. Rev. C* **52**, R23 (1995).
 [20] H. Koura, M. Uno, T. Tachibana, and M. Yamada, *Nuclear Physics A* **674**, 47 (2000).
 [21] G. F. Bertsch and D. Bingham, *Phys. Rev. Lett.* **119**, 252501 (2017).
 [22] V. R. Pandharipande, J. G. Zabolitzky, S. C. Pieper, R. B. Wiringa, and U. Helmbrecht, *Phys. Rev. Lett.* **50**, 1676 (1983).
 [23] V. R. Pandharipande, S. C. Pieper, and R. B. Wiringa, *Phys. Rev. B* **34**, 4571 (1986).
 [24] R. A. Aziz, V. P. S. Nain, J. S. Carley, W. L. Taylor, and G. T. McConville, *J. Chem. Phys.* **70**, 4330 (1979).
 [25] M. Bender, P.-H. Heenen, and P.-G. Reinhard, *Rev. Mod. Phys.* **75**, 121 (2003).
 [26] M. Brack, C. Guet, and H.-B. Hkansson, *Physics Reports* **123**, 275 (1985).
 [27] M. Dutra, O. Lourenço, J. S. Sá Martins, A. Delfino, J. R. Stone, and P. D. Stevenson, *Phys. Rev. C* **85**,

035201 (2012).
 [28] M. Kortelainen, T. Lesinski, J. Moré, W. Nazarewicz, J. Sarich, N. Schunck, M. V. Stoitsov, and S. Wild, *Phys. Rev. C* **82**, 024313 (2010).
 [29] A. Rios, A. Polls, and W. H. Dickhoff, *Phys. Rev. C* **89**, 044303 (2014).
 [30] V. M. Galitski and A. B. Migdal, *Sov. Phys. JETP* **7**, 96 (1958).
 [31] M. Piarulli, L. Girlanda, R. Schiavilla, A. Kievsky, A. Lovato, L. E. Marcucci, S. C. Pieper, M. Viviani, and R. B. Wiringa, *Phys. Rev. C* **94**, 054007 (2016).
 [32] M. Piarulli, A. Baroni, L. Girlanda, A. Kievsky, A. Lovato, E. Lusk, L. E. Marcucci, S. C. Pieper, R. Schiavilla, M. Viviani, and R. B. Wiringa, *Phys. Rev. Lett.* **120**, 052503 (2018).
 [33] A. Baroni, R. Schiavilla, L. E. Marcucci, L. Girlanda, A. Kievsky, A. Lovato, S. Pastore, M. Piarulli, S. C. Pieper, M. Viviani, and R. B. Wiringa, *Phys. Rev. C* **98**, 044003 (2018).
 [34] B. S. Pudliner, V. R. Pandharipande, J. Carlson, and R. B. Wiringa, *Phys. Rev. Lett.* **74**, 4396 (1995).
 [35] G. Hagen, T. Papenbrock, A. Ekström, K. A. Wendt, G. Baardsen, S. Gandolfi, M. Hjorth-Jensen, and C. J. Horowitz, *Phys. Rev. C* **89**, 014319 (2014).
 [36] D. Lonardoni, I. Tews, S. Gandolfi, and J. Carlson, “Nuclear and neutron-star matter from local chiral interactions,” (2019), [arXiv:1912.09411 \[nucl-th\]](https://arxiv.org/abs/1912.09411).
 [37] C. Drischler, K. Hebeler, and A. Schwenk, *Phys. Rev. Lett.* **122**, 042501 (2019).
 [38] C. Mahaux and R. Sartor, “Single-particle motion in nuclei,” in *Advances in Nuclear Physics*, edited by J. W. Negele and E. Vogt (Springer US, Boston, MA, 1991) pp. 1–223.
 [39] M. H. Mahzoon, R. J. Charity, W. H. Dickhoff, H. Dusan, and S. J. Waldecker, *Phys. Rev. Lett.* **112**, 162503 (2014).
 [40] W. H. Dickhoff, R. J. Charity, and M. H. Mahzoon, *J. of Phys. G: Nucl. and Part. Phys.* **44**, 033001 (2017).
 [41] D. Baye, *Physics Reports* **565**, 1 (2015), the Lagrange-mesh method.
 [42] A. Carbone, A. Cipollone, C. Barbieri, A. Rios, and A. Polls, *Phys. Rev. C* **88**, 054326 (2013).
 [43] J. Carlson, S. Gandolfi, F. Pederiva, S. C. Pieper, R. Schiavilla, K. E. Schmidt, and R. B. Wiringa, *Rev. Mod. Phys.* **87**, 1067 (2015).
 [44] S. C. Pieper and R. B. Wiringa, *Annu. Rev. Nucl. Part. S.* **51**, 53 (2001), <https://doi.org/10.1146/annurev.nucl.51.101701.132506>.
 [45] R. Machleidt and D. R. Entem, *Physics Reports* **503**, 1 (2011).
 [46] G. Hagen, M. Hjorth-Jensen, G. R. Jansen, R. Machleidt, and T. Papenbrock, *Phys. Rev. Lett.* **109**, 032502 (2012).
 [47] M. C. Atkinson, H. P. Blok, L. Lapikás, R. J. Charity, and W. H. Dickhoff, *Phys. Rev. C* **98**, 044627 (2018).
 [48] M. C. Atkinson and W. H. Dickhoff, *Phys. Lett. B* **798**, 135027 (2019).
 [49] M. C. Atkinson, M. H. Mahzoon, M. A. Keim, B. A. Bodelon, C. D. Pruitt, R. J. Charity, and W. H. Dickhoff, *Phys. Rev. C* **101**, 044303 (2020).
 [50] R. Machleidt, F. Sammarruca, and Y. Song, *Phys. Rev. C* **53**, R1483 (1996).
 [51] R. B. Wiringa, V. G. J. Stoks, and R. Schiavilla, *Phys. Rev. C* **51**, 38 (1995).
 [52] D. R. Entem and R. Machleidt, *Phys. Rev. C* **68**, 041001

- (2003).
- [53] K. Bennaceur and J. Dobaczewski, *Computer Physics Communications* **168**, 96 (2005).
 - [54] O. Hen, G. A. Miller, E. Piasetzky, and L. B. Weinstein, *Rev. Mod. Phys.* **89**, 045002 (2017).
 - [55] B. P. Abbott *et al.* (LIGO Scientific Collaboration and Virgo Collaboration), *Phys. Rev. Lett.* **119**, 161101 (2017).
 - [56] R. B. Wiringa, R. Schiavilla, S. C. Pieper, and J. Carlson, *Phys. Rev. C* **89**, 024305 (2014).
 - [57] J. Dobaczewski, W. Nazarewicz, and M. V. Stoitsov, *The European Physical Journal A* **15**, 21 (2002).
 - [58] A. Ekström, G. R. Jansen, K. A. Wendt, G. Hagen, T. Papenbrock, B. D. Carlsson, C. Forssén, M. Hjorth-Jensen, P. Navrátil, and W. Nazarewicz, *Phys. Rev. C* **91**, 051301 (2015).
 - [59] H. Dussan, S. J. Waldecker, W. H. Dickhoff, H. Muther, and A. Polls, *Phys. Rev. C* **84**, 044319 (2011).
 - [60] V. M. Lebedev, N. V. Orlova, O. I. Serikov, and S. A. V., *Izv. Rossiiskoi Akademii Nauk, Ser.Fiz.* **70**, 1645 (2006).
 - [61] K. Wienhard, G. Clausnitzer, and G. Hartmann, *Z. Physik* **256**, 457 (1972).
 - [62] I. E. Dayton and G. Schrank, *Phys. Rev.* **101**, 1358 (1956).
 - [63] J. Swint, A. Barnard, T. Clegg, and J. Weil, *Nuclear Physics* **86**, 119 (1966).
 - [64] S. Kobayashi, S. Motonaga, Y. Chiba, K. Katori, A. Stricker, T. Fujisawa, and T. Wada, *Journal of the Physical Society of Japan* **29**, 1 (1970), <https://doi.org/10.1143/JPSJ.29.1>.
 - [65] Girod, M., Nguyen Van Sen, Longequeue, J.P., and Tsan Ung Chan, *J. Phys. France* **31**, 125 (1970).
 - [66] M. Ieiri, H. Sakaguchi, M. Nakamura, H. Sakamoto, H. Ogawa, M. Yosol, T. Ichihara, N. Isshiki, Y. Takeuchi, H. Togawa, T. Tsutsumi, S. Hirata, T. Nakano, S. Kobayashi, T. Noro, and H. Ikegami, *Nuclear Instruments and Methods in Physics Research Section A: Accelerators, Spectrometers, Detectors and Associated Equipment* **257**, 253 (1987).
 - [67] Z. An, Q. Chen, Y.-H. Cheng, D.-J. Shen, and G. Guo, *Chinese Phys. Lett.* **20**, 478 (2003).
 - [68] J. K. Dickens, D. A. Haner, and C. N. Waddell, *Phys. Rev.* **132**, 2159 (1963).
 - [69] L. N. Blumberg, E. E. Gross, A. VAN DER Woude, A. Zucker, and R. H. Bassel, *Phys. Rev.* **147**, 812 (1966).
 - [70] V. I. Grantsev, V. A. Konfederatenko, O. F. Nemets, R. G. Ofengenden, B. A. Rudenko, M. V. Sokolov, and B. G. Struzhko, *Ukrainskii Fizichnii Zhurnal* **28**, 506 (1983).
 - [71] A. Rush, E. Burge, and D. Smith, *Nuclear Physics A* **166**, 378 (1971).
 - [72] J. R. Comfort, S. M. Austin, P. T. Debevec, G. L. Moake, R. W. Finlay, and W. G. Love, *Phys. Rev. C* **21**, 2147 (1980).
 - [73] J. Emmerson, J. Madden, C. Johnson, N. Middlemas, A. Clegg, and W. Williams, *Nuclear Physics* **77**, 305 (1966).
 - [74] V. M. Hannen, K. Amos, A. M. van den Berg, R. K. Bieber, P. K. Deb, F. Ellinghaus, D. Frekers, M. Hagemann, M. N. Harakeh, J. Heyse, M. A. de Huu, B. A. M. Krüsemann, S. Rakers, R. Schmidt, S. Y. van der Werf, and H. J. Wörtche, *Phys. Rev. C* **67**, 054320 (2003).
 - [75] V. Comparat, R. Frascaria, N. Marty, M. Morlet, and A. Willis, *Nuclear Physics A* **221**, 403 (1974).
 - [76] H. O. Meyer, P. Schwandt, W. W. Jacobs, and J. R. Hall, *Phys. Rev. C* **27**, 459 (1983).
 - [77] A. Johansson, U. Svanberg, and P. E. Hodgson, *Arkiv Fys.* **19**, 541 (1961).
 - [78] A. Ingemarsson, O. Jonsson, and A. Hallgren, *Nuclear Physics A* **319**, 377 (1979).
 - [79] M. Ibaraki, M. Baba, T. Miura, Y. Hirasawa, Y. Nauchi, H. Nakashima, S.-I. Meigo, O. Iwamoto, S. Tanaka, N. Hirakawa, and T. Hiroishi, *Jour. of Nucl. Sci. and Tech. Suppl.* **2**, 204 (2002).
 - [80] R. White, R. Lane, H. Knox, and J. Cox, *Nuclear Physics A* **340**, 13 (1980).
 - [81] G. Haouat, J. Lachkar, J. Sigaud, Y. Patin, and F. Cou, *Nuclear Science and Engineering* **65**, 331 (1978), <https://doi.org/10.13182/NSE78-A27161>.
 - [82] D. W. Glasgow, F. O. Purser, H. Hogue, J. C. Clement, K. Stelzer, G. Mack, J. R. Boyce, D. H. Epper-son, S. G. Buccino, P. W. Lisowski, S. G. Glendinning, E. G. Bilpuch, H. W. Newson, and C. R. Gould, *Nuclear Science and Engineering* **61**, 521 (1976), <https://doi.org/10.13182/NSE76-A14488>.
 - [83] N. Olsson, B. Trostell, and E. Ramström, *Nuclear Physics A* **496**, 505 (1989).
 - [84] J. H. Osborne, F. P. Brady, J. L. Romero, J. L. Ullmann, D. S. Sorenson, A. Ling, N. S. P. King, R. C. Haight, J. Rapaport, R. W. Finlay, E. Bauge, J. P. Delaroche, and A. J. Koning, *Phys. Rev. C* **70**, 054613 (2004).
 - [85] J. Klug, J. Blomgren, A. Ataç, B. Bergenwall, A. Hildebrand, C. Johansson, P. Mermod, L. Nilsson, S. Pomp, U. Tippawan, K. Elmgren, N. Olsson, O. Jonsson, A. V. Prokofiev, P.-U. Renberg, P. Nadel-Turonski, S. Dangtip, P. Phansuke, M. Österlund, C. Le Brun, J. F. Lecolley, F. R. Lecolley, M. Louvel, N. Marie-Noury, C. Schweitzer, P. Eudes, F. Haddad, C. Lebrun, A. J. Koning, and X. Ledoux, *Phys. Rev. C* **68**, 064605 (2003).
 - [86] L. Sydow, S. Vohl, S. Lemaitre, P. Niesen, K. Nyga, R. Reckenfelderbumer, G. Rauprich, and H. gen. Schieck, *Nuclear Instruments and Methods in Physics Research Section A: Accelerators, Spectrometers, Detectors and Associated Equipment* **327**, 441 (1993).
 - [87] R. Craig, J. Dore, G. Greenlees, J. Lowe, and D. Watson, *Nuclear Physics* **79**, 177 (1966).
 - [88] S. Kato, K. Okada, M. Kondo, A. Shimizu, K. Hosono, T. Saito, N. Matsuoka, S. Nagamachi, K. Nisimura, N. Tamura, K. Imai, K. Egawa, M. Nakamura, T. Noro, H. Shimizu, K. Ogino, and Y. Kadota, *Nuclear Instruments and Methods* **169**, 589 (1980).
 - [89] W. Bauhoff, S. Collins, R. Henderson, G. Shute, B. Spicer, V. Officer, K. Amos, I. Morrison, D. Devins, D. Friesel, and W. Jones, *Nuclear Physics A* **410**, 180 (1983).
 - [90] C. D. Roper, W. Tornow, R. T. Braun, Q. Chen, A. Crowell, D. G. Trotter, C. R. Howell, F. Salinas, R. Setze, R. L. Walter, Z. Chen, H. Tang, and Z. Zhou, *Phys. Rev. C* **72**, 024605 (2005).
 - [91] P. Hillman and G. H. Stafford, *Il Nuovo Cimento (1955-1965)* **3**, 633 (1956).
 - [92] J. F. Dicello and G. Igo, *Phys. Rev. C* **2**, 488 (1970).
 - [93] J. J. H. Menet, E. E. Gross, J. J. Malanify, and A. Zucker, *Phys. Rev. C* **4**, 1114 (1971).
 - [94] A. Auce, A. Ingemarsson, R. Johansson, M. Lantz, G. Tibell, R. F. Carlson, M. J. Shachno, A. A. Cowley, G. C. Hillhouse, N. M. Jacobs, J. A. Stander, J. J. v. Zyl, S. V. Förtsch, J. J. Lawrie, F. D. Smit, and G. F.

- Steyn, [Phys. Rev. C **71**, 064606 \(2005\)](#).
- [95] W. P. Abfalterer, F. B. Bateman, F. S. Dietrich, R. W. Finlay, R. C. Haight, and G. L. Morgan, [Phys. Rev. C **63**, 044608 \(2001\)](#).
- [96] P. J. Dimbylow, [Physics in Medicine and Biology **25**, 637 \(1980\)](#).
- [97] H. de Vries, C. W. de Jager, and C. de Vries, [Nucl. Data Tables **36**, 495 \(1987\)](#).
- [98] I. Sick, J. B. Bellicard, J. M. Cavedon, B. Frois, M. Huet, P. Leconte, P. X. Ho, and S. Platchkov, [Phys. Lett. B **88**, 245 \(1979\)](#).